A 60 GHz Radio-Over-Fiber Network Architecture for Seamless Communication With High Mobility

Nikos Pleros, Konstantinos Vyrsokinos, Kostas Tsagkaris, and Nikolaos D. Tselikas

Abstract—We demonstrate a 60 GHz broadband picocellular Radio-over-Fiber network architecture that enables seamless connectivity for highly mobile end-users. Its seamless communication capabilities arise by the supported handover scheme that relies on a novel Moving Extended Cell (MEC) concept. MEC exploits user-centric virtual groups of adjacent cells that transmit the same data content to the user and utilizes a switch mechanism for restructuring the virtual multi-cell area according to the user's mobility pattern, so that a virtual antenna group moves together with the mobile user. We present the theoretical formulation for MEC and show that it can provide zero packet loss and call dropping probability values in high-rate wireless services for a broad range of mobile speeds up to 40 m/sec, independently of the fiber link distances. We also demonstrate the physical layer network architecture and switch mechanism both for a RoF network with a single 60 GHz radio frequency (RF) over each wavelength, as well as for a RoF configuration supporting simultaneous multi-RF channel transmission over each optical wavelength. The performance of the multi-RF-over-λ network implementation is evaluated via simulations showing successful 100 Mb/s radio signal transmission over fiber links longer than 30 km. To this end, MEC can enable seamless connectivity and bandwidth guarantees in 60 GHz picocellular RoF networks being also capable of serving multiple users over the same wavelength in a RF frequency-division-multiplexed (FDM) approach.

Index Terms—60 GHz wireless communications, indoor wireless, moving extended cell, pico-cellular networks, radio-over-fiber, seamless communication, vehicle communication.

I. INTRODUCTION

RADIO-OVER-FIBER (RoF) networks have emerged as a new and promising communication paradigm for delivering broadband wireless access services at 60 GHz relying on the synergy between fixed optical and mobile millimeter (mm)-waveband technologies [1]. The potential of RoF networks to enable Gb/s data rate provision to mm-wave wireless end-users has been already confirmed by several experimental research attempts [1]–[3], whereas they have also demonstrated impressive capabilities towards supporting different wireless technologies

N. Pleros is with the Computer Science Department, Aristotle University of Thessaloniki, Thessaloniki, Greece (e-mail: npleros@csd.auth.gr).

K. Vyrsokinos is with the School of Electrical and Computer Engineering, National Technical University of Athens, Zografou, GR 15773 Athens, Greece (e-mail: kvyrs@cc.ece.ntua.gr).

K. Tsagkaris is with the Department of Technology Education and Digital Systems, University of Piraeus, Athens, Greece, (e-mail: ktsagk@unipi.gr).

N. D. Tselikas is with the Department of Telecommunications Science and Technology, University of Peloponnese, Tripoli, Greece (e-mail: ntsel@uop.gr).

[3]–[7] and both indoor [8], [9] and outdoor mobile applications [10].

However, the 60 GHz RoF network perspective has to overcome innate limitations enforced by the 60 GHz frequency band in order to ensure a seamless mobile communication environment. The strong air-propagation losses and the line-of-sight requirements of the 60 GHz signals usually restrict cell radii to a few tens of meters [8]–[10] when low antenna directivity is employed, yielding inevitably to picocellular configurations with small overlapping areas between neighboring cells. As such, only a small time window is available for successfully completing a handover process when a Mobile User (MU) crosses the cell boundaries and moves to the neighboring cell, implying that only low moving speeds can be accommodated without losing connection. This time window is further reduced in indoor application scenarios, where the additional attenuation induced by walls and furniture leads to radio cells that are typically confined in a single room, and to directional and even narrower overlap areas formed only around doors and windows [8], [9]. The situation becomes even worse due to corner effect phenomena, where a sharp turn of the MU moving from one room to another can cause sudden loss of the line-of-sight with the present Remote Antenna Unit (RAU), impeding the completion or even the initiation of a handover process [8].

So far, seamless communication concepts for picocellular wireless networks have mainly involved three-level hierarchical architectures for multi-cell groups [11] or Virtual Cell Network configurations [12], [13]. However, seamless connectivity in 60 GHz picocellular RoF networks has been only recently addressed utilizing Dynamic Capacity Allocation (DCA) mechanisms both in the physical and network layers. Physical layer DCA has been presented employing wavelength routing approaches [2], whereas indoor [8], [9] and outdoor [10] RoF seamless environments have relied on static Extended Cell (EC) and Virtual Cellular Zones (VCZ), respectively. Both EC structures and VCZs exploit predefined, static groups of adjacent cells in order to increase cell overlapping areas and provide reduced call dropping values. A dynamically adaptable cellular structure of "moving cells" has been also proposed for providing broadband access to train passengers [14], requiring however the a priori knowledge of the train's velocity and direction in order to acquire synchronization between the cellular adaptation mechanism and the passenger's speed, restricting in this way its application to mobility scenarios of limited mobility randomness.

In this article, we demonstrate a novel concept for seamless communication supporting high end-user mobility in broadband 60 GHz Radio-over-Fiber networks irrespective of the

user's mobility pattern. Our scheme relies on a capacity reallocation mechanism for reconfiguring the Extended Cells so as to form user-centric Moving Extended Cell (MEC) structures that follow the user's mobility pattern. In this way, the end-user is always surrounded by a certain number of grouped cells transmitting concurrently the same user-specific data over the same radio frequency enabling in this way seamless communication conditions for truly random mobility and velocity patterns. The MEC scheme is mathematically formulated and results from the performance evaluation reveal zero packet loss and call dropping probabilities for user velocities up to 40 m/sec irrespective of the overlapping region between neighboring cells. We also present the physical layer network architecture for the realization of 2.5 Gb/s downlink connection over a single 60 GHz radio frequency using the MEC approach. Finally, we propose for the first time a hybrid Frequency Division Multiplexing (FDM)/Wavelength Division Multiplexing (WDM) network architecture supporting the delivery of multiple RF channels in the 60 GHz frequency band over the same wavelength, increasing in this way the number of possible wireless users for a given number of wavelengths whilst retaining a seamless environment. Successful downlink transmission of 8 RF frequencies each one carrying 100 Mb/s is demonstrated through physical layer simulations for a multi-user scenario employing the MEC scheme. Finally, the proposed seamless communication approach is entirely performed and controlled by an optical switch located at the Central Office (CO) of the RoF network retaining in this way all the scalability advantages offered by the consolidation of network functionalities at the CO of RoF architectures.

The rest of the paper is organized as follows. Section II describes the concept of MEC and presents its mathematical analysis. Section III involves the performance evaluation of a RoF network when MEC is employed and compares its results with the simple case of inter-cellular handover. Section IV demonstrates the physical layer switch architectures and respective results for the realization of MEC in RoF networks with both single- or multiple RF-over-λ frequencies. Finally, Section V introduces alternative MEC configurations and discusses possible applications.

II. THE MOVING EXTENDED CELL CONCEPT

A. Introduction

Fig. 1 provides a schematic representation of the MEC concept depicting a MU in a picocellular network configuration. Each cell corresponds to a specific RAU and the gray area indicates the group of cells that comprise an Extended Cell transmitting the same user-specific data content over the same radio frequency. As shown in Fig. 1(a), the Extended Cell involves the user's cell and the six surrounding cells ensuring connectivity for all possible directions when the user leaves his/her current cell #4. However in the case of user's entry in a new cell, the Extended Cell is recomposed so as to form a new user-centric seven-cell group following the user's motion. This is clearly illustrated in Fig. 1(b), where the MU leaves cell #4 and moves into cell #7. Upon receiving the beacon signal of cell #7, the initial Extended Cell is reconfigured so that cell #7 becomes the
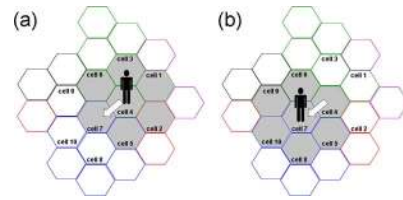

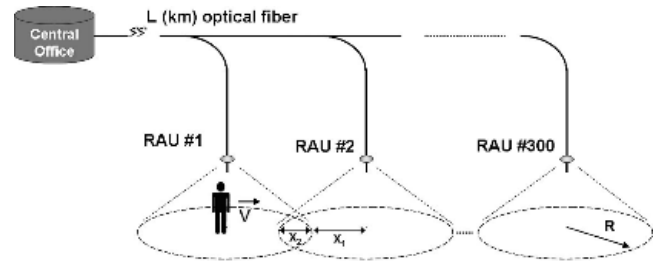Fig. 1. The moving extended cell concept.

Fig. 2. The network configuration used for the performance analysis of the MEC concept.

new central cell, resulting to a new Extended Cell formation that consists of cells #3, #4, #6, #7, #8, #9 and #10, releasing the capacity of cells #1, #2 and #5. To this end, the Extended Cell is always formed around user's current location and is adaptively restructured when the user enters a new cell. As a result, the end-user is continuously surrounded by cells that transmit the same data content, offering in this way seamless communication conditions for all possible subsequent movements [15].

It should be noted that the 7-cell EC structure can be easily adjusted when cells with less than six adjacent cells are considered by following a more generic MEC formulation that relies on EC structures encompassing $m+1$ cells, with m denoting the number of neighboring cells. To this end, the MEC formed for one user in a generic network topology can eventually incorporate a different number of cells depending on the user's location and the associated number of neighbor-cells. This can be enabled by taking advantage of the centralized network topology knowledge provided by the CO in order to allocate the required number of MEC cells in each MEC reconfiguration process.

Fig. 2 shows the network configuration considered for the mathematical formulation of MEC. 300 picocells formed by respective RAUs are placed on a straight line and are connected to the CO via optical fibers. When concentrating on a single MU transition between two neighboring cells, the fiber links between the two adjacent RAUs can be assumed to have the same length L since the cell radius R is only a few tens of meters, whilst L is in the km-range and as such $R \ll L$. The axial length of the overlapping region between adjacent cells is denoted as x_2, whereas x_1 stands for the difference R-x_2. The beacon signals are emitted periodically at time intervals of T_b and are considered synchronized among all RAUs taking advantage of the common control management enabled by the CO. The MU can move with a constant velocity V along the line formed by the cell centers and lies initially at the center of RAU#1 cell, implying an initial EC that includes RAU#1 and RAU#2 cells.

Let us assume that beacon signal transmission begins at $t = t_0$, the MU enters the overlapping area between RAU#1 and

RAU#2 cells at the moment t_1, and RAU#2 emits its next beacon frame at the moment t_h. The MU will receive this beacon signal if it is still in the RAU#2 cell at the moment t_h, and it will respond via an ACK signal to RAU#2 announcing its presence and initiating the Extended Cell reconfiguration process. In this way, a new Extended Cell consisting of RAU#2 and RAU#3 cells will be formed. A call drop upon leaving RAU#2 cell will occur only if the end-user has transit RAU#2 cell before t_h, implying that he will have crossed a total distance of 2R in a time interval of $t_h - t_1$. This results to a call drop velocity cut-off condition provided by

$$V = \frac{2R}{(t_h - t_1)}. \tag{1}$$

During user's transition from RAU#1 to RAU#2 cell, no packet loss will be experienced since both cells transmit the same data content being part of the initial Extended Cell. The MU will exhibit packet losses only in the case of leaving RAU#2 cell and entering RAU#3 cell prior to the completion of the Extended Cell reconfiguration process, i.e., before RAU#3 starts the emission of the user-specific data signal. The time T_{total} needed for completing the Extended Cell reconfiguration procedure is provided by

$$T_{total} = T_{proc} + \Delta t_{update} + \frac{L}{\frac{c}{n}} \tag{2}$$

where T_{proc} is the processing time of the CO switch, Δt_{update} is the time required following the beacon reception for informing the CO about the Extended Cell reconfiguration request, and $L/c/n$ is the time needed for the data packets to propagate through the fiber link from the CO to RAU#3, with c being the speed of light and n denoting the fiber refractive index. The CO is updated about the user's Extended Cell reconfiguration request via the ACK message sent by the MU through RAU#2, yielding a Δt_{update} that corresponds to the propagation delay of the ACK signal. This propagation delay includes the time needed to travel through the wireless link between the MU and RAU#2 and the time required to propagate through the fiber link between RAU#2 and the CO.

If $\Delta t_{\#2}$ is the time required by the user for crossing the RAU#2 cell boundaries after receiving the RAU#2 beacon frame, packet loss will equal zero as long as $T_{total} < \Delta t_{\#2}$ since RAU#3 will start the data packet transmission while the user is still in the RAU#2 cell. However, if $T_{total} > \Delta t_{\#2}$ then packets that cross the CO during a total time T_{loss} will be lost. The value of T_{loss} depends on whether the CO becomes updated prior to the user's exit from RAU#2 cell or not. If the user loses connection to RAU#2 before the CO becomes updated and data packets are routed to RAU#3, the packets contained in the link between the CO and the end-user by the time of exiting RAU#2 cell, as well as the subsequent packets that will cross the CO before its update, will not reach the MU. The succeeding packets crossing the CO before its update correspond to a time interval of $\Delta t_{update} - \Delta t_{\#2}$. However, in case the CO becomes updated before the user's exit, data packets will already be in the link between CO and RAU#3 by the time of crossing the RAU#2 cell boundaries and as such

they will be received by the MU through RAU#3. To this end, T_{loss} is provided by

$$T_{loss} = \frac{L}{\frac{c}{n}} + \frac{R}{c \cdot \cos\theta} + T_{proc} + (\Delta t_{update} - \Delta t_{\#2}),$$
$$\text{if } \Delta t_{\#2} < \Delta t_{update} \tag{3}$$

$$T_{loss} = \frac{L}{\frac{c}{n}} + \frac{R}{c \cdot \cos\theta} + T_{proc} - (\Delta t_{\#2} - \Delta t_{update}),$$
$$\text{if } \Delta t_{update} < \Delta t_{\#2} \tag{4}$$

with θ denoting the angle formed between the MU and the RAU with respect to the horizontal plane. A detailed mathematical treatment for the call drop and packet loss expressions in MEC is provided in [15].

Taking into account that packets are transmitted at a packet rate $r = S/B$ with B and S denoting their Constant Bit Rate (CBR) and packet size, respectively, including any possible guardbands, then the total packet loss in number of packets can be easily calculated using the expression

$$packetloss = T_{loss} \cdot r \tag{5}$$

in case the MU has completed its last packet reception process when exiting RAU#2 cell, and by the relationship

$$packetloss = T_{loss} \cdot r + 1 \tag{6}$$

if the MU is within a reception process whilst crossing the cell boundaries [16].

III. SIMULATION RESULTS

A C++ simulation model for the RoF network shown in Fig. 2 has been developed in order to evaluate the network's performance when employing the MEC concept and compare it with the general simple case scenario that employs the conventional hard-handover approach for user transitions between single pic-ocells [16]. For the purposes of our analysis, the simple message exchange scheme involving two possible situations for the packet loss calculation has been considered: the first situation refers to the reception of the beacon frame by the MU before the data packet is sent by the RAU, and the second one corresponds to beacon reception after the RAU sends the data packet [16].

The signal and network parameters used in the complete series of simulations carried out have the same values both for the MEC and the simple-case handover approach, being: $R = 20\,\text{m}$, $T_b = 1\,\text{sec}$ and a continuous CBR data flow traffic profile with data packet size of 210 bytes. Average packet loss and call dropping probability values have been calculated as the average values of a set of more than 100 independent simulations, with each simulation run having a run-time of less than 30 sec using an Intel Core2 Duo CPU at 2.4 GHz with 3 GB RAM. Processing times of a few μsecs at the CO have been incorporated in the T_{loss} expression. In order to avoid any correlation, the moments that the RAUs start sending beacons, the MU starts moving and the data traffic starts being sent, are randomly chosen within the interval [0.0, 1.0] secs.

Fig. 3 illustrates the average call dropping probability per user transition as a function of the user's velocity for both cases of simple handover and MEC, considering five possible values for the axial overlapping distance x_2 within the range [1 m, 5.35 m].
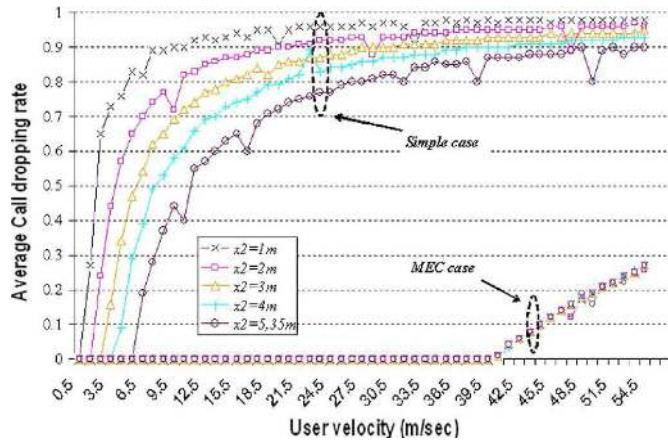
Fig. 3. Average call dropping probability per user transition versus user velocity in the simple case and in the MEC approach for a cell radius of $R = 20\,m$.

Fig. 4. Average packet loss versus optical fiber link length for three different bit-rates in the simple case scenario.

The value $x_2 = 5.35\,m$ was chosen so as to correspond to the overlapping area among the circumscribed circles of hexagonal-type cells given by $x_2 = \left(2 - \sqrt{3}\right) \cdot R$. In the simple handover case, the call dropping probability is zero until the user's velocity reaches the value x_2/T_b. This suggests a maximum speed limit for retaining connectivity that depends on x_2 and is restricted to pedestrian velocities even for an overlapping distance of 5.35 m. When the user velocity becomes greater than its x_2-dependent upper limit, the call dropping probability increases very quickly, exceeding 20% for speed values greater than 10 m/sec.

In the case of MEC, the call dropping probability is independent of x_2 and is zero for the complete range of user velocities below 40 m/sec. This is a result of dynamically rearranging the user-centric Extended Cell by establishing a new user connection in all possible next destination cells upon entering a new cell area, preparing seamless conditions for all possible subsequent movements. In this way, the time interval being available for initiating the Extended Cell reconfiguration equals the new cell's transit time and is independent of the actual overlapping area between adjacent cells, resulting to enhanced flexibility in network planning and to seamless conditions even for vehicle speeds. Beyond 40 m/sec, call drops are gradually increasing at a slower rate than in the simple handover case, yielding values greater than 20% only for speeds beyond 50 m/sec, i.e., 180 km/h.

Figs. 4 and 5 depict the packet loss values per user transition obtained in the simple handover case and in MEC, respectively, for various fiber link lengths $L = \{1, 2, 10, 30\}$ km and for three different packet bit rates $B = \{100, 144, 200\}$ Mb/s. As shown in Fig. 4, the packet loss in the simple handover case is independent of mobile speed and increases almost linearly with increasing fiber length and bit rate. For High-Definition TV services at 144 Mbps, an average packet loss of two packets is obtained when considering a fiber link of $L = 2$ km that could eventually correspond to a 60 GHz indoor RoF infrastructure for a small conference center or airport. In case the same service is delivered over an extended RoF network with 30 km fiber links, the exhibited packet loss increases significantly approaching a number of 25 lost data packets.

The situation is greatly improved in the case of MEC. As Fig. 5 reveals, packet loss will be zero irrespective of the data
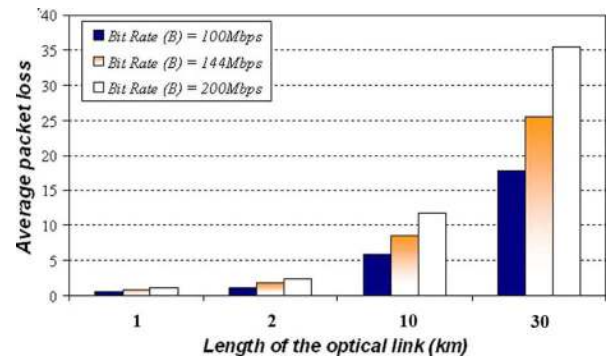
rate and the fiber link length between the CO and the RAU as long as the MU moves with a velocity lower than 40 m/sec. The packet loss increases beyond the zero level only when the user's speed exceeds 40 m/sec. Beyond 40 m/sec, the average packet loss depends on MU's velocity and is almost linearly related to L and B when comparing MT motions of the same velocity. However, average packet loss remains very low in all possible combinations of L, B and V and is almost always less than 0.3, reaching its 0.9 upper limit only in the case of $V = 40$ m/sec, $L = 30$ km and $B = 200$ Mb/s.

These low values are a result of triggering the MEC procedure prior to entering the new cell, indicating that the user will continue to listen to its current RAU after sending the ACK message. As such, data packets are lost only if the user leaves its current cell before the Extended Cell rearrangement has been completed. However, the total time required for the new RAU to start the data packet emission, as provided by (2), is below the msec range. Within this short time, the end-user moves only a few centimeters away, implying that the MU has to be located very close to the cell boundaries when requesting an EC reconfiguration in order to experience packet losses, severely limiting in this way the packet loss incidence possibilities. This is also the reason that the packet loss values are maximized when the user moves with a velocity of 40 m/sec, which corresponds to a propagation distance equal to the entire cell within a beacon time period. This speed value results to periodic pattern for the user's intra-cell positions of higher repetition frequency than by other velocities, increasing the probabilities for user locations close to the cell boundaries when receiving the beacon signal.

IV. PHYSICAL LAYER ARCHITECTURE

Following the performance analysis of the MEC concept in terms of call dropping probability and packet loss values, we propose a first optical physical layer network architecture that enables the realization of the MEC approach. We demonstrate an optical switching architecture for implementing MEC in the CO, emphasizing on providing the complete MEC reconfigurability directly in the optical domain. The proposed network architecture exploits WDM technology so that each RAU is associated with a dedicated wavelength necessitating the use of a minimum number of wavelength channels equal to the number of RAUs employed in the network. In this way, every cell is served by a specific λ allowing for the MU's data transfer to a new cell by simply switching the data to the wavelength serving the new cell.
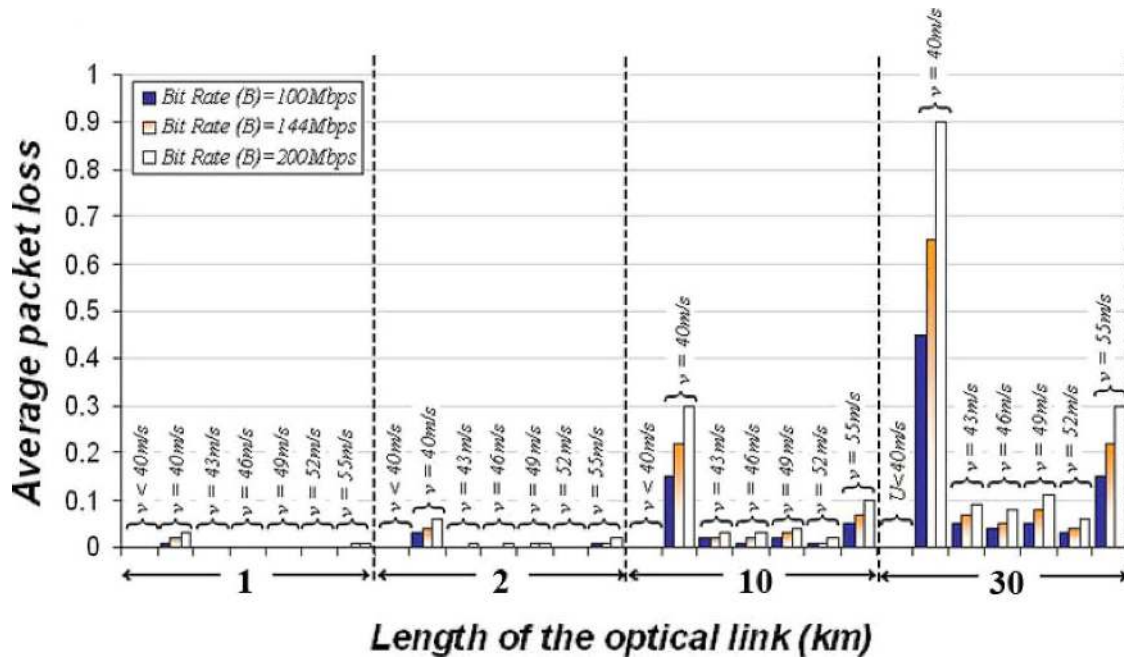
Fig. 5. Average packet loss versus optical fiber link length for three different bit-rates and different user velocities in the case of MEC.

A. Single 60 GHz RF -Over-λ Network

This network approach utilizes a single 60 GHz RF carrier frequency modulated on every optical wavelength and carrying data at up to 2.5 Gb/s data rates, so that that every MU uses a wireless connection at 60 GHz. The physical layer configuration for a network using M wavelengths and being capable of serving a total number of N mobile users is depicted in Fig. 6(a). By considering a 7-cell Extended Cell structure, each MU's data will be carried at a 60 GHz RF carrier, which will be in turn superimposed on the 7 wavelengths that correspond to the 7 cells forming the MU's current EC. In order to avoid wavelength collision and RF interference effects, only one user can be located in every 7-cell group implying that the network can in total support a number of $N = M/7$ users.

The CO employs M lasers each one emitting at a different wavelength $\lambda_1, \lambda_2, \ldots, \lambda_M$. The laser outputs feed an optical $M \times N$ switching matrix that comprises M $1 \times N$ optical switches interconnected to N $M \times 1$ Arrayed Waveguide Grating (AWG) multiplexers (MUX#1...MUX#N). An electrical control plane is used for driving the optical switching matrix and determining its state. Each AWG output signal enters an optical LiNbO3 modulator [5], which is driven by a microwave signal obtained by mixing a 60 GHz sinusoidal signal and a 2.5 Gb/s data signal generated by an electrical Pseudo-Random Bit Sequence (PRBS) generator. The N modulated output signals, each one corresponding to the data required by every respective wireless user, are launched into a $N \times 1$ optical combiner and enter the same optical single mode fiber (SMF) link of length L. At the output of the SMF, an additional $1 \times M$ AWG is used for demultiplexing the optical wavelengths and transmitting each λ to its specific RAU. In order to avoid undesirable signal degradation due to dispersion phenomena in the SMF, the central wavelength of each AWG passband is mistuned with respect to the incoming data wavelength so as to suppress the lower 60 GHz frequency band and yield a Single-Side-Band

(SSB) modulated data signal at every RAU [17]. Every RAU consists of a simple high-speed photodiode that provides an electrical 60 GHz modulated signal at its output exploiting coherent beating phenomena between the carrying wavelength and its 60 GHz sub-carrier. The electrical output signal is then filtered in a 2.5 GHz Bandpass-Filter (BPF) centered at 60 GHz and is emitted into the air by means of a microwave antenna. The inset of Fig. 6(b) shows the receiver setup when used only for the optical link performance evaluation, where the microwave transmitting antenna has been replaced with a microwave 60 GHz-to-baseband downconversion scheme.

In this network layout, the complete MEC reconfiguration functionality is offered by the $M \times N$ optical switch. The λ_k wavelength entering its respective $1 \times N$ switch can be switched to any of the S_N switch output ports depending on the MU that it will serve. The n-th output port S_n of each $1 \times N$ switch is assigned for serving user#n, suggesting that it has to guide the signal to the k-th input port of the n-th AWG MUX so as to subsequently act as the input signal into MOD#n. According to these assignments, a 7-cell MEC around the user#n can be implemented by properly configuring the electronic control plane so as to force exact 7 wavelengths to enter their respective input ports at the n-th AWG MUX. If the MU enters a new cell, the new MEC is formed simply by modifying the state of the $1 \times N$ switches so as to insert three new wavelengths into the n-th AWG whilst blocking the entrance of the respective three wavelengths that were used for the previous MEC formation.

The physical layer MEC reconfiguration process with its respective optical spectra is illustrated in more detail in Fig. 7. Fig. 7(a) shows two mobile users located in adjacent Extended Cells and the aggregate spectrum involving all necessary wavelengths that propagates along the RoF fiber link. User#1 forms an EC consisting of the cells assigned to λ_1-λ_7 wavelengths, whereas user#2 forms an EC that comprises λ_8-λ_{14} wavelengths. Fig. 7(b) depicts the situation where user#2 enters
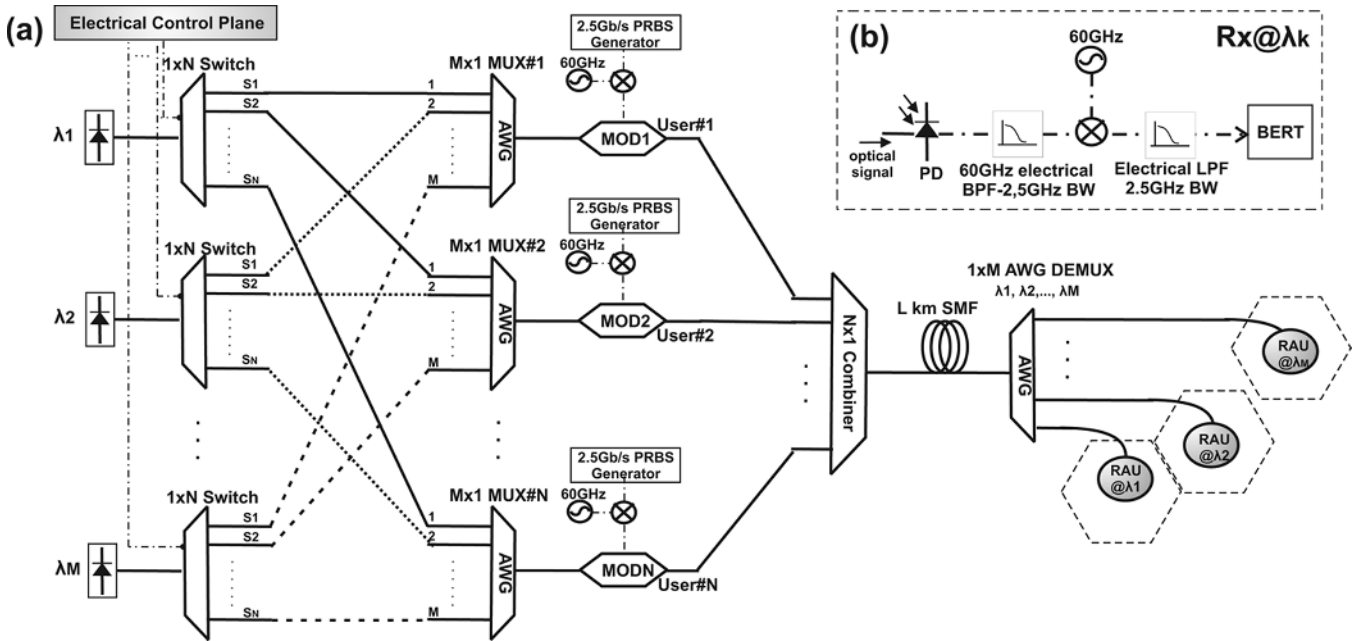
Fig. 6. (a) The physical layer RoF CO switch and network architecture for the implementation of MEC. (b) The receiver setup used for the optical link performance evaluation at the λ_k-cell.
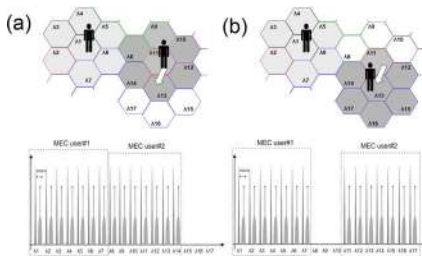

Fig. 7. (a) Two neighboring MECs formed around respective users and the corresponding optical spectrum, and (b) the new MEC formations and the respective optical spectrum after one user moves into the new cell λ_{13}.

TABLE I
ALTERNATIVE CO OPTICAL SWITCH IMPLEMENTATIONS (SOURCE: [14])

Switch Type	Switching time
SOA, electro-optic	5 nsec
Acousto-optic	3 µsec
MEMS, bubble	10 msec

the cell corresponding to the wavelength λ_{13}. In this case, the new user-centric EC requires the user's#2 data to be carried by λ_{11}-λ_{17} wavelengths, implying that the λ_{15}-λ_{17} wavelengths will be switched through the $M \times N$ optical switching matrix so as to enter the modulator MOD#2. At the same time, λ_8-λ_{10} wavelengths will be blocked from entering MOD#2 releasing their capacity.

Given that the data emission RF frequency is the same in every single cell within the 7-cell EC, this frequency is used by the MU for the whole call duration following an approach similar to Single Frequency Network (SFN) architectures [13], [22]. This restriction prohibits the overlapping between the ECs formed around two MUs. If, for example, user#2 of Fig. 7(b) would enter λ_{14} cell instead of λ_{13}, the cell served by λ_6 would be common to both ECs formed by user#1 and user#2, suggesting that the 60 GHz subcarrier of λ_6 wavelength should carry information of both MUs. In order to avoid call blocking for one of the two users, specific MEC reconfiguration policies should be employed, which however are beyond the scope of the present work. An alternative way for enabling the presence of multiple wireless users within the same MEC would be the

incorporation of effective Medium Access Control (MAC) protocols [18], [21] that could in principle exploit Time Division Multiplexed (TDM) access schemes. In this way, the 2.5 Gb/s capacity would be shared among the users and each MU would be served within a specific time slot of the corresponding wavelength.

The $1 \times N$ switches can be realized by a variety of optical technologies summarized in Table I, depending on the desired switching speed and cost-effectiveness. It should be noted than even the use of the lower rate MEMS switches having a 10 msec switching time renders a seamless communication environment when MEC is employed. Call dropping probability follows the curve for the MEC case shown in Fig. 3, as this property does not depend on the characteristic switching times. The respective packet loss values for various user velocities and fiber link distances for a 100 Mb/s continuous traffic stream per user and a 5.35 m overlapping area between neighboring cells are shown in Fig. 8. For MU speeds below 40 m/sec packet loss equals zero, whilst for user speeds exceeding 40 m/sec packet loss values remain always lower than 15. It should be noted that packet loss appears to be almost independent of the fiber link distance since the contribution of the μsec-scale propagation times in the total T_{loss} expression, as provided by (3) and (4), is negligible compared to the 10 msec MEMS switch processing time. The advantages of MEC even with MEMS-based optical switches are
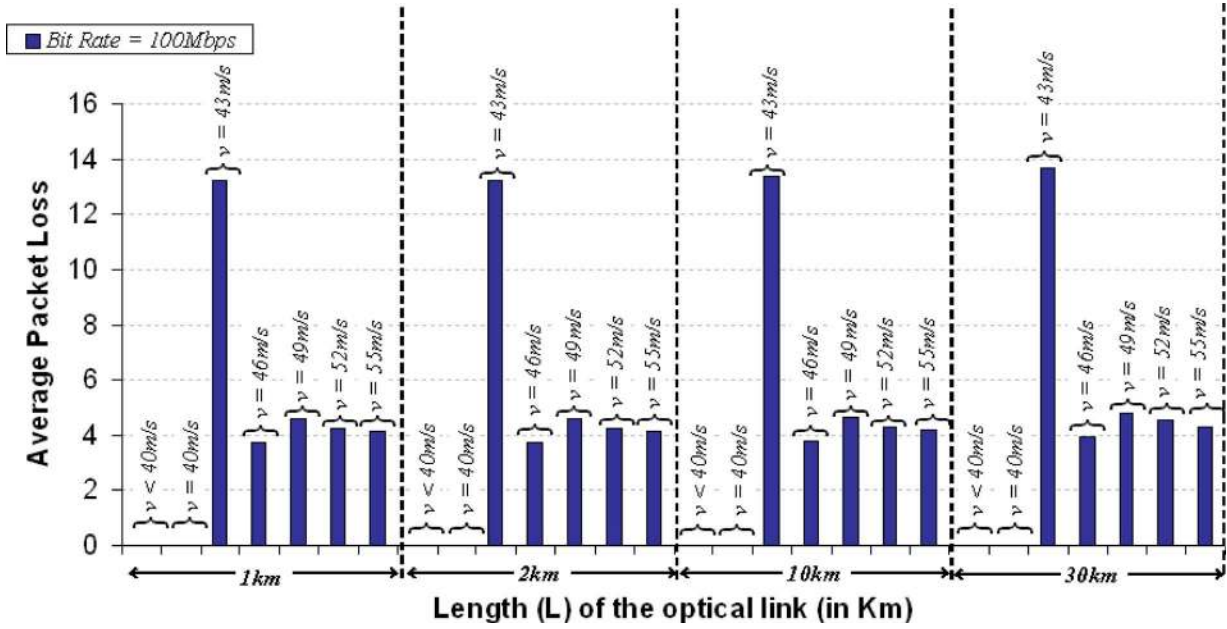
Fig. 8. Packet loss versus fiber link for different user speeds when an optical switch with 10 msec processing times is used at the CO.

even more highlighted when comparing with the case where no MEC approach is employed and a simple handover scheme is used in every cell transit, which yields packet loss values greater than 600.

B. Hybrid 60 GHz-Band FDM/WDM RoF Network

In order to increase the number of possible wireless users for a given number of M available wavelengths and to provide guaranteed wireless bandwidths in a RoF network supporting MEC, we introduce a two-dimensional perspective into the utilization of the available spectrum proposing for the first time a hybrid FDM/WDM approach for 60 GHz RoF network architectures. Besides allocating capacity through 60 GHz carrier frequency over an optical wavelength, we present an 8 RF channel allocation scheme within the 60 GHz band of every λ and demonstrate simulation-based results in a seamless communication RoF architecture relying on MEC. In this way, the capacity being available for one user in each cell is designated by a unique (λ, f) pair originating by the matrix multiplication of

$$\begin{pmatrix} \lambda_1 \\ \lambda_2 \\ \vdots \\ \lambda_M \end{pmatrix} \cdot (f_1 \ f_2 \cdots f_8). \tag{7}$$

To this end, each 7-cell MEC formed around a single user#i requires the allocation of (λ_k, f_i) pairs for seven different k values, indicating that each MEC can now support a number of simultaneously present MUs equal to the number of wireless carrier frequencies f_i supported by the network.

Fig. 9 illustrates the optical switching matrix for the implementation of a hybrid FDM/WDM RoF network. It employs again a laser bank of M lasers each emitting light at a different wavelength. Every laser output is then split into 8 equal parts via an 1×8 optical splitter and each part is inserted into a respective

$M \times N$ optical switch that is identical to the switch depicted in Fig. 6(a). To this end, a total number of $8 \, M \times N$ optical switches is now required, so that each switch will be responsible for the optical capacity allocation in the respective group of wireless users that exploit the same f_i RF carrier frequency. The N output ports of an optical switch enter N respective $LiNbO_3$ modulators that correspond to a group of N users. In every user group, each modulator is driven by the microwave sum of a sinusoidal RF signal at f_i and a 100 Mb/s data signal provided by a PRBS generator, with $i = 1, 2, \ldots, 8$. The modulator outputs are again combined in a $N \times 1$ optical combiner forming $8N$ optical signals that are subsequently launched into the common SMF link via an 8×1 combiner. The electronic control plane is again responsible for setting the state of the $1 \times N$ optical switches so as to allow only a maximum number of 7 different wavelengths to enter the modulator of a specific user in a single RF user group.

Given that each RAU is again considered to be assigned to a specific wavelength, the RoF network configuration after signal aggregation at the output of the CO is similar to the network layout depicted in Fig. 6(a). Fig. 10 shows the RAU setup as it has been used for the optical link performance evaluation. A photodiode is used for converting the optical into an electrical data signal at f_i carrier frequency, which is then downconverted and electrically filtered prior being detected and characterized at the bit error rate tester (BERT).

The physical layer performance of the 8 RF channel/WDM RoF network supporting seamless connectivity by employing MEC has been evaluated through simulations based on the commercial VPI Physical Layer version 7.5 simulation package. A total number of 17 wavelengths in the 1550 nm region with a wavelength spacing of 200 GHz and an output power of 2 mW per wavelength was used, whereas the 8 RF carrier frequencies had a frequency spacing of 300 MHz ranging from 58.8 to 60.9 GHz. The 100 Mb/s data signal carried by each RF channel had a Non-Return-to-Zero (NRZ) $2^{23} - 1$ PRBS content and was
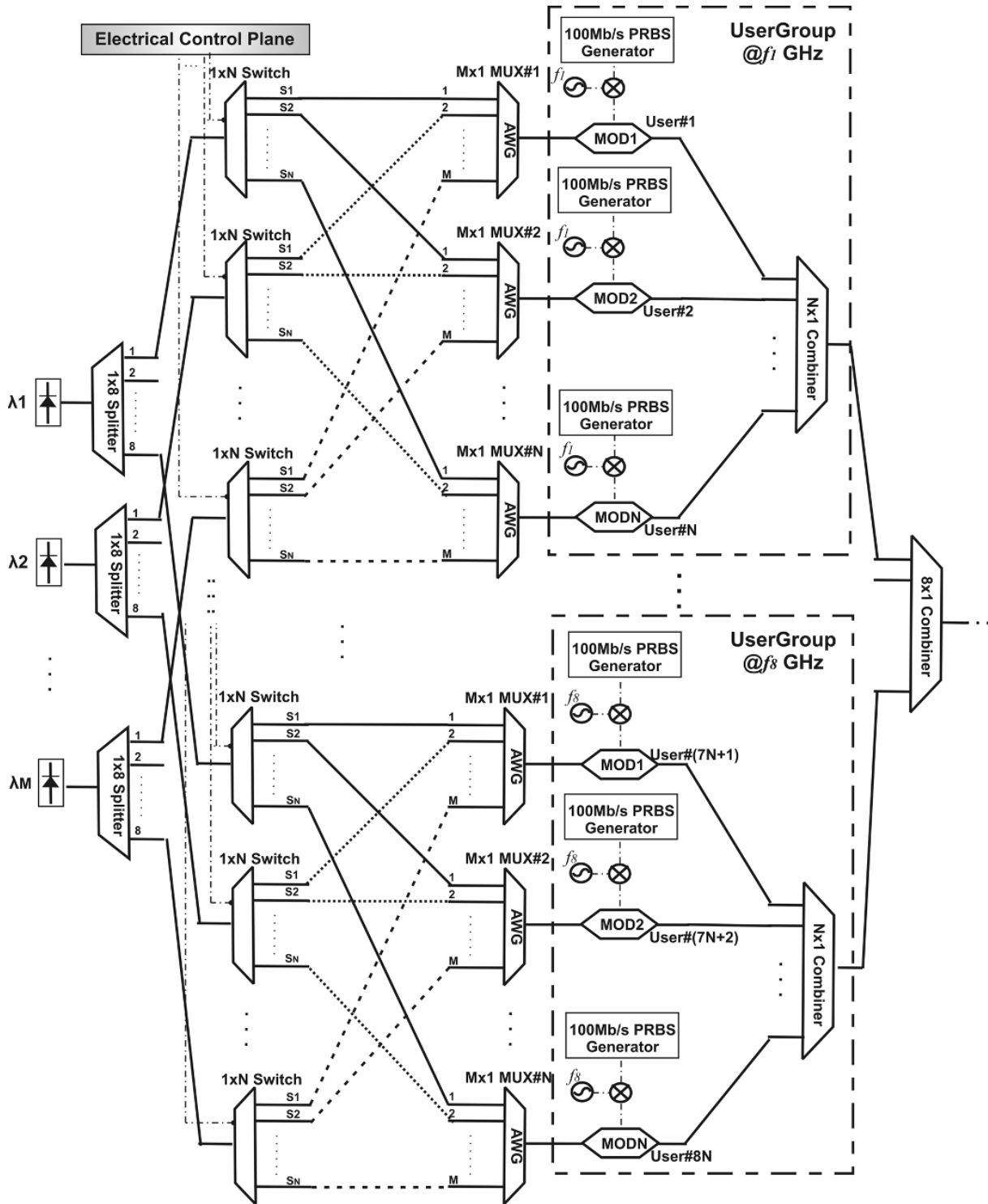
Fig. 9. The CO optical switch layout for enabling MEC in a hybrid FDM/WDM RoF network with 8 RF frequency channels.

set to have an initial rms timing jitter of 0.5 nsec. The AWGs employed at the DEMUX stage at the output of the L km SMF link had a trapezoid shape with 3 dB bandwidth of 120 GHz and 25 dB of 200 GHz and the mismatch of the center frequency of the filter with respect to the original input wavelengths was 32 GHz so as to ensure symmetrical transmission characteristics through the AWG for every incoming wavelength and its higher 60 GHz frequency band. The total optical insertion losses of the

switch for every single wavelength channel were 31 dB considering insertion loss parameters close to that of real systems for every individual component: a 1×16 MEMS-based optical switch with 3 dB per port losses, an AWG with 4 dB insertion losses, 3 dB losses for the optical modulator and splitter/combiner implementations based on 3 dB coupler arrangements. An Erbium-Doped Fiber Amplifier (EDFA) of 30 dB gain was used directly at the output of every single wavelength source resulting
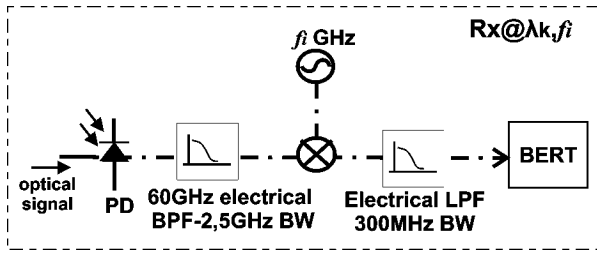
Fig. 10. The receiver setup used for the optical link performance evaluation of the f_i–user at the λ_k-cell.
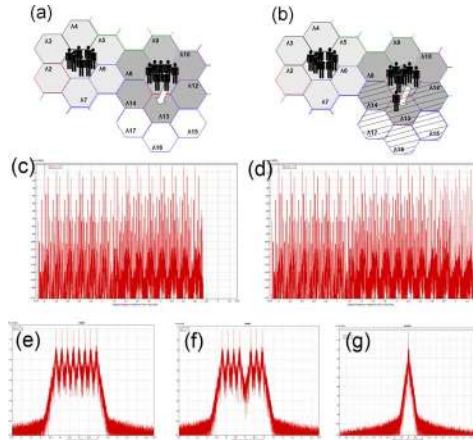

Fig. 11. (a) Two neighboring MEC structures each one having 8 MU at their central cell, (b) the MEC configurations when one MU enters a new cell, (c) the aggregate optical spectrum corresponding to the two MECs of Fig. 11(a), (d) the respective aggregate optical spectrum for the two MECs of Fig. 11(b), (e), and (f) the microwave spectrum around the 60 GHz band in the λ_9 cell prior and after the MU's movement, respectively, and (g) the microwave spectrum around the 60 GHz band at λ_{15} cell. The RF spectra in (c) and (d) are centered around 194.7 THz having a frequency axis division of 200 GHz. The spectra in (e), (f), and (g) are centered at 60 GHz with a frequency division of 500 MHz.

finally to a total power of 1.5 mW for every channel at the common port of the final 8×1 combiner. These values indicate that the feasibility of our system for use also in practical implementations is in principle not prohibited by the total insertion losses as they can be compensated by simple EDFA-based amplification stages. Moreover, a SOA-based switch implementation would further reduce the total insertion losses of the switch taking advantage of the optical gain offered by the SOA devices.

Fig. 11 depicts two indicative scenarios before and after a MU enters a new cell, i.e., for two different statically configured optical switching matrix states. Fig. 11(a) depicts two adjacent 7-cell MEC formations with 8 MUs located at each MEC's central cell associated with the λ_1 and λ_{11} wavelengths, respectively. The respective optical spectrum is shown in Fig. 11(c) involving all relevant wireless information on λ_1-λ_{14} wavelengths. Fig. 11(b) illustrates the case when the MU using the $f_5 = 60$ GHz carrier frequency enters the λ_{13} cell, leading to a new MEC formation around this user. This new user-centric MEC employs the cells depicted by the diagonal black lines including cells λ_{15}-λ_{17} and releasing the f_5 capacity at cells λ_8-λ_{10}. Given that the MEC structures for the other 15 users remain unaffected, the total optical spectrum will now incorporate all 17 wavelengths, as shown in Fig. 11(d).
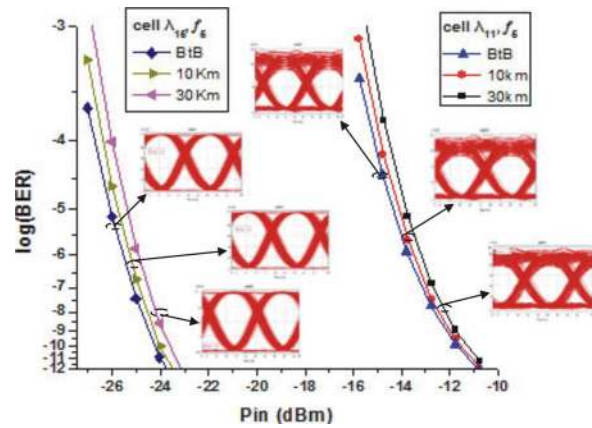

Fig. 12. BER measurements showing the respective eye diagrams as insets.

Fig. 11(e) and (f) show in more detail the microwave spectra within the 60 GHz subcarrier band around λ_9 prior and after the f_5-user's movement, respectively. All 8 RF frequency carriers are contributing to the λ_9 modulation before the f_5-user leaves this cell, but after the f_5-user has moved into cell λ_{13} the f_5 data subcarrier is not any more present around λ_9. At the same time, the f_5 data subcarrier becomes the single modulating signal for wavelength λ_{15} as depicted in Fig. 11(g), as well as for the wavelengths λ_{16} and λ_{17}.

Fig. 12 depicts the BER measurements and the respective eye diagrams obtained for the 100 Mb/s f_5-user's data at the two cells λ_{11} and λ_{15} using the receiver configuration of Fig. 10 and for two different network fiber links of L $=$ 10 km and L $=$ 30 km. In both cells, a small power penalty of 0.3 dB and 0.8 dB is obtained for the 10 km and 30 km distance, respectively. The power penalty of 11.5 dB between the corresponding BER curves of λ_{15} and λ_{11} cells owe to the increased number of RF channels carried by λ_{11} with respect to λ_{15}. The seven RF-over-λ_{11} channels produce significant nonlinear beating terms spaced at 300 MHz when entering the receiver photodiode, transferring a significant amount of energy to the new generated frequency harmonics. This becomes evident also through the corresponding eye diagrams that show a higher signal degradation at the mark level compared to the eye diagrams of λ_{15} cell. In the λ_{15} cell, only the f_5 RF channel is used, suggesting that no nonlinear RF beating cross-terms will be generated at the photodiode. In this way, no energy will be lost and a lower receiver sensitivity is required for error-free performance. The power penalty induced on the f_5-channel by different number of RF channels carried on a single wavelength for a BER value of 10^{-12} is illustrated in Fig. 13, indicating clearly that the power penalty increases nonlinearly with the number of RF channels even for the BtB case and that only a very small additional overhead is obtained by the transmission of this signal in the 30 km fiber link.

V. DISCUSSION

The call dropping probability and packet loss characteristics of the MEC concept make it an attractive seamless connectivity perspective providing several benefits both for indoor as well
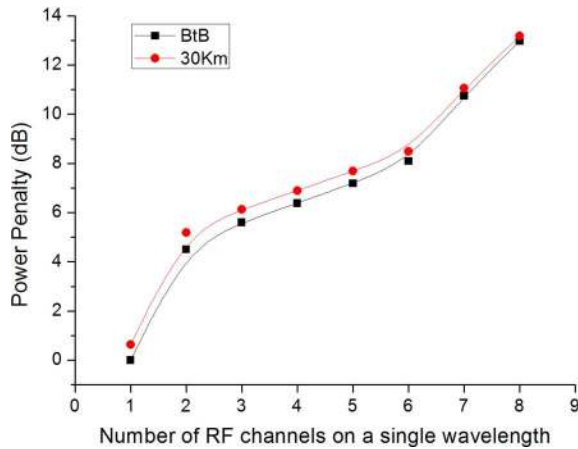
Fig. 13. Power penalty versus number of RF channels carried on a single wavelength for a BER of 10^{-12} considering the BtB curve for a singe RF channel as the 0 dB power penalty reference point.

as for outdoor high mobility wireless environments. The x_2 insensitivity indicates that MEC can effectively mitigate indoor corner-effect phenomena relaxing line-of-sight requirements at 60 GHz and offering certain advantages in the in-building communication networks. In this scenario, corner effect phenomena will be avoided since a MU will always be in the central cell of an Extended Cell structure retaining connectivity even when moving out of a room and making a sharp turn. MEC leads also to zero packet losses for user velocities below the cut-off condition irrespective of the network dimensions and the associated fiber lengths, indicating its potential to enable highly reliable RoF indoor communications with seamless mobility, for example in big airport and conference centres.

MEC can also support broadband applications with high end-user mobility, as verified by the low call dropping probability and packet loss values even for 200 Mb/s data rates and speeds up to 50 m/sec that render it suitable for outdoor vehicle communication systems. Given also that packet loss remains small even for network links > 30 km, the adoption of the MEC concept can enable broadband mm-wave-over-optical wireless services in road vehicle communications supporting extended network dimensions. In this scheme, one-dimensional optical fiber link infrastructure could be employed along the highway or the railway interconnecting COs spaced at several tens of kms and offering radio coverage to running vehicles. Such a 1-D network scenario would require just 2 adjacent cells instead of 7 for forming an Extended Cell, suggesting reduced bandwidth overhead in the MEC formation and allowing for increased maximum number of users. Moreover, given that high mobility is the rule in highways or railways, MEC's flexibility allows for a cell rearrangement so as to involve the user's cell and two additional cells being in the front of the moving vehicle, which would double the maximum user's velocity before a call drop incidence.

To this end, the MEC concept and the proposed, associated mm-waveband RoF architecture can be utilized as an effective broadband wireless communication platform with picocellular-level radio coverage resolution, enhancing flexibility and area granularity in cellular networks. Despite its requirement for a number of wavelengths in order to form a single

user-centric MEC, the number of connected users can increase for a given total number of wavelengths being available at the network's CO by exploiting hybrid FDM/WDM techniques or effective MAC protocol schemes. In addition, the number of cells required for constituting an Extended Cell in certain network topologies can be lower than seven, as in the case of road vehicle applications that require only two-cell groups across a single direction, or in the case of in-building environments if taking into account the building's architectural constraints with respect to possible user motions. Finally, it should be noted that the MEC scheme is not restricted to RoF physical layer architectures but it can be applied to any type of picocellular single-frequency wireless networks provided that an appropriate signalling and control mechanism is utilized in order to effectively initiate and complete the MEC reconfiguration process.

As the MEC concept relies on single wireless frequency approaches where the MU utilizes the same RF channel for the whole call duration, specific policy schemes can be adopted to protect call blocking due to undesirable collisions. Multipath effects like frequency selective fading and Intersymbol Interference (ISI) as well as frequency interference effects caused by the concurrent transmission of the same data over the same frequency in an Extended Cell can be mitigated by using orthogonal frequency division multiplexing (OFDM) modulation schemes for the RF carrier frequencies employing hybrid OFDM/WDM RoF techniques [8], [9], [19] in combination with appropriate guardtime intervals [22] or antenna array techniques [13] used in SFN implementations. Finally, despite the MEC concept presented in this work has considered only downstream traffic, it is in principle compatible with traditional uplink configurations [20] by incorporating adaptive MAC protocols for providing services to multiple users being simultaneously at the same cell [21].

VI. CONCLUSION

We have demonstrated a handover scheme and its associated physical layer network architecture for providing seamless broadband wireless communication with high end-user mobility in 60 GHz RoF networks irrespective of the user's mobility pattern. Our scheme employs a SFN radio frequency approach and a handover mechanism that is based on a novel Moving Extended Cell concept introducing reconfigurability in user-centric Extended Cell structures so that they can move together with the MU. A physical layer MEC-enabling implementation for the CO optical switch is presented and its physical layer performance for a hybrid FDM/WDM RoF network supporting 100 Mb/s wireless CBR data traffic is demonstrated. The proposed MEC handover functionality is performed entirely by the optical switch located at the CO retaining in this way all scalability advantages arising by the centralized RoF network architectures. Our scheme yields seamless communication regardless of the overlapping area size between adjacent cells and for mobile speeds up to 40 m/sec. To this end, it can effectively mitigate corner effect phenomena and high-mobility applications, rendering 60 GHz RoF networks suitable for both indoor pedestrian and outdoor vehicle wireless communications.

REFERENCES

[1] M. Sauer, A. Kobyakov, and J. George, "Radio over fiber for picocellular network architectures," *J. of Lightwave Technol.*, vol. 25, no. 11, pp. 3301–3320, Nov. 2007.

[2] J. J. V. Olmos, T. Kuri, and K. Kitayama, "Dynamic reconfigurable WDM 60-GHz millimeter-waveband radio-over-fiber access network: Architectural considerations and experiment," *J. Lightwave Technol.*, vol. 25, no. 11, pp. 3374–3380, Nov. 2007.

[3] H. S. Chung, S. H. Chang, J. D. Park, M.-J. Chu, and K. Kim, "Transmission of multiple HD-TV signals over a wired/wireless line millimeter-wave link with 60 GHz," *J. Lightwave Technol.*, vol. 25, no. 11, pp. 3413–3418, Nov. 2007.

[4] Q. Chang *et al.*, "A PON system providing triple play service based on a single dual-parallel Mach-Zehnder modulator," presented at the 33rd Eur. Conf. Opt. Commun. (ECOC) 2007, Berlin, Germany, Sep. 2007.

[5] Q. Chang, H. Fu, and Y. Su, "Simultaneous generation and transmission of downstream multiband signals and upstream data in a bidirectional radio-over-fiber system," *IEEE Photon. Technol. Lett.*, vol. 20, pp. 181–183, Feb. 2008.

[6] M. Bakaul, A. Nirmalathas, C. Lim, D. Novak, and R. Waterhouse, "Hybrid multiplexing of multiband optical access technologies towards an integrated DWDM network," *IEEE Photon. Technol. Lett.*, vol. 18, pp. 2311–2313, Nov. 2006.

[7] M. Toycan, M. P. Thakur, and S. D. Walker, "Optical network architecture for UWB range extension beyond a single complex of cells," presented at the 33rd Eur. Conf. Opt. Commun. (ECOC) 2007, Berlin, Germany, Sep. 2007.

[8] B. L. Dang, V. Prasad, I. Niemegeers, M. Garcia Larrode, and A. Koonen, "Toward a seamless communication architecture for in-building networks at the 60 GHz band," in *Proc. 31st IEEE Conf. Local Comp. Networks (LCN)*, Tampa, FL, 2006.

[9] B. L. Dang, M. Garcia Larrode, R. Venkatesha Prasad, I. Niemegeers, and A. M. J. Koonen, "Radio-over-Fiber based architecture for seamless wireless indoor communication in the 60 GHz band," *Comput. Commun.*, vol. 30, pp. 3598–3613, 2007.

[10] H. B. Kim, M. Emmelmann, B. Rathke, and A. Wolisz, "A radio over fiber network architecture for road vehicle communication systems," in *Proc. Veh. Technol. Conf.*, 2005, vol. 5, pp. 2920–2924.

[11] R. Ghai and S. Singh, "An architecture and communication protocol for picocellular networks," *IEEE Pers. Commun. Mag.*, vol. 1, no. 3, pp. 36–46, 1994.

[12] H. J. Kim and J. P. Linnartz, "Virtual cellular network: A new wireless communications architecture with multiple access ports," *Wireless Pers. Commun.*, vol. 10, no. 3, pp. 287–307, 1999.

[13] M. Flament, A. Svensson, and J. M. Cioffi, "Performance of 60 GHz virtual cellular networks using multiple receiving antennas," *Wireless Pers. Commun.*, vol. 23, no. 1, pp. 15–29, 2002.

[14] B. Lannoo, D. Colle, M. Pickavet, and P. Demeester, "Radio-over-fiber-based solution to provide broadband internet access to train passengers," *IEEE Commun. Mag.*, vol. 45, no. 2, pp. 56–62, Feb. 2007.

[15] N. Pleros, K. Tsagkaris, and N. D. Tselikas, "A moving extended cell concept for seamless communication in 60 GHz radio-over-fiber networks," *IEEE Commun. Lett.*, vol. 12, no. 11, pp. 852–854, Nov. 2008.

[16] L. Peters, I. Moerman, B. Dhoedt, and P. Demeester, "Impact of the access network topology on the handoff performance," *Wireless Netw.*, vol. 13, pp. 203–220, 2007.

[17] J. Ma, J. Yu, C. Yu, X. Xin, J. Zeng, and L. Chen, "Fiber dispersion influence on transmission of the optical millimeter-waves generated using LN-MZM intensity modulation," *J. Lightw. Technol.*, vol. 25, no. 11, pp. 3244–3256, Nov. 2007.

[18] B.-L. Dang, V. Prasad, and I. Niemegeers, "On the MAC protocols for radio over fiber networks," presented at the IEEE Int. Conf. Consum. Electron. (ICCE) 2006, Hanoi, Vietnam, Oct. 2006.

[19] H. Kim *et al.*, "Radio-over-fiber system for TDD-based OFDMA wireless communication systems," *J. Lightw. Technol.*, vol. 25, no. 11, pp. 3419–3427, Nov. 2007.

[20] X. Zhang, B. Liu, J. Yao, K. Wu, and R. Kashyap, "A novel millimeter-wave-band radio-over-fiber system with dense wavelength-division multiplexing bus architecture," *IEEE Trans. Microw. Theory Tech.*, vol. 54, no. 2, pp. 929–937, Feb. 2006.

[21] G. Kalfas, P. Nikolaidis, N. Pleros, and G. I. Papadimitriou, "A radio-over-fiber network with MAC protocol that provides intelligent and dynamic resource allocation," presented at the IEEE/LEOS Summer Topicals 2009 Conf., Newport Beach, CA, Jul. 2009.

[22] A. Mattsson, "Single frequency networks in DTV," *IEEE Trans. Broadcast.*, vol. 51, no. 4, pp. 413–422, Dec. 2005.

Nikos Pleros joined the faculty of the Department of Informatics, Aristotle University of Thessaloniki, Greece, in September 2007, where he is currently serving as a Lecturer. He received the Diploma and the Ph.D. degree in electrical and computer engineering from the National Technical University of Athens (NTUA) in 2000 and 2004, respectively.

From 2005 until September 2007, he was a Teaching and Research Associate at NTUA. His research interests include multi-wavelength cw and pulsed laser sources for WDM/OTDM and high data-rate telecommunications, respectively, all-optical signal processing and digital logic modules, all-optical packet/burst/label switching systems and architectures, semiconductor-based switching devices, optical wireless access and Radio-over-fiber systems and networks, optical interconnects and biophotonics. He has more than 55 archival journal publications and conference presentations including invited contributions. He has participated in several EC-funded FP6 and FP7 research projects both in the fields of optical cnetworks and biophotonics.

Dr. Pleros has received the 2003 IEEE/LEOS Graduate Student Fellowship granted to 12 Ph.D. candidates worldwide and was also awarded the 15th prize in the Greek Mathematical Olympiad in 1993. He is a member of the IEEE Photonics Society, the IEEE ComSoc, and the Optical Society of America (OSA).

Konstantinos Vyrsokinos, photograph and biography not available at the time of publication.

Kostas Tsagkaris received the Diploma and the Ph.D. degree from the School of Electrical Engineering and Computer Science, National Technical University of Athens (NTUA), Athens, Greece, in 2000 and 2004, respectively. In 2005, he received the Ericsson's Award of Excellence in Telecommunications for his Ph.D. thesis.

He has been involved in many international and national research projects, especially working on the areas of design, management, and optimization of communications networks. Since January 2004, he has been a Senior Research Engineer in the Department of Digital Systems, University of Piraeus, Athens. Since September 2005, he has been an Adjunct Lecturer in the undergraduate and postgraduate programs of the same department. His current interests are in the design, management and performance evaluation of wireless broadband and cognitive networks, optimization algorithms, learning techniques and software engineering. He has published more than 55 papers in international journals and refereed conferences.

Dr. Tsagkaris is a member of the ACM and a member of the Technical Chamber of Greece. He is also a voting member of IEEE SCC 41 and of IEEE P1900.4 WG, where he has served as Technical Editor.

Nikolaos D. Tselikas, photograph and biography not available at the time of publication.